

Cascade Reactions in Tunable Lamellar Micro-Mesopores for C=C Bond Coupling and Hydrocarbon Synthesis

Fan Lin,^[a] Junyan Zhang,^[b] Dongxia Liu,^[b] and Ya-Huei (Cathy) Chin*^[a]

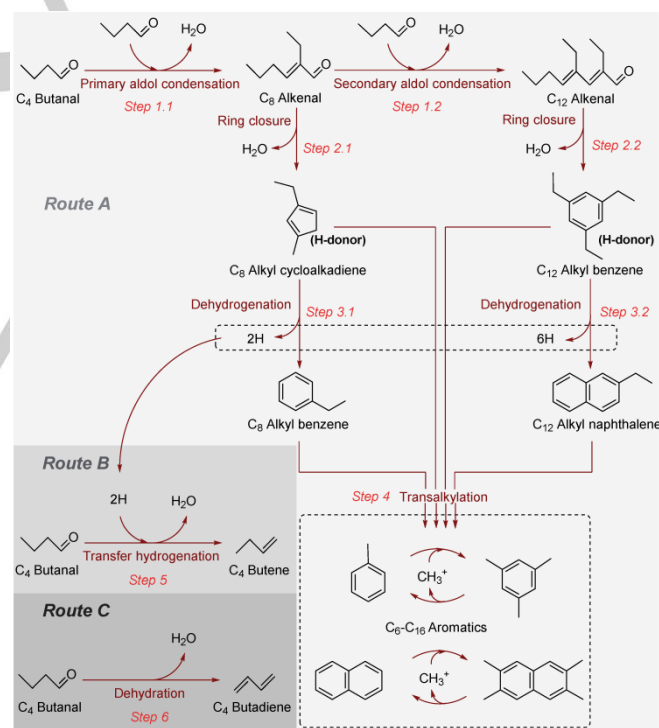
Abstract: Two-dimensional MFI zeolite nanosheets (2D-MFI) contain Brønsted acid sites partially confined at the intercept between micro- and meso-pores (H_{pc}^+). These acid sites exhibit exceptional reactivities and stabilities for C=C bond coupling and ring closure reactions that transform light aldehydes to aromatics. These sites are much more effective than those confined within the micropores of MFI crystallites and those unconfined on $H_4SiW_{12}O_{40}$ clusters or mesoporous aluminosilicate Al-MCM-41. The partially confined site environment solvates and stabilizes the transition states of the kinetically-relevant steps during aromatization.

Microporous acidic materials (H-MFI, H-FAU, etc.) are effective catalysts for industrial hydrocarbon synthesis, which includes cracking, isomerization, and transalkylation reactions.^[1] They also catalyze oxygen removal and C=C bond coupling of functionalized oxygenates, converting them into alkenes and aromatics.^[2] These materials, however, suffer from rapid deactivation, because their pores of molecular dimensions not only promote shape selective catalysis, but also trap and convert heavier products into coke, which then blocks the accessibility of reactants to the Brønsted acid sites (H^+).^[3] Circumventing this deactivation issue is of industrial importance, attained here by designing a new class of Brønsted acid catalysts for stable and selective hydrocarbon and oxygenate conversions.

Herein, we introduce hierarchical MFI zeolite materials (denoted as 2D-MFI) with individual crystallites containing two-dimensional lamellar layers of micro- and meso-pores (Fig. 1a) as effective Brønsted acid catalysts for synthesizing aromatics from aldehydes. These hierarchical zeolite lamellae contain micro- and meso-pore intercepts, at which partially confined Brønsted acid sites (H_{pc}^+ , subscript *pc* denotes partially confined) reside. These partially confined H_{pc}^+ sites are selective for the conversion of aldehydes to aromatics than the unconfined sites on polyoxometalate clusters (H_{uc}^+ , subscript *uc* denotes unconfined) and the confined H_c^+ sites within the micro-pores of conventional three-dimensional MFI zeolite (H_c^+ , subscript *c* denotes confined, in 3D-MFI). The unique location of the H_{pc}^+ sites also allows for more effective transport and removal of large aromatic products. The more stable transition state afforded by the partially confined H_{pc}^+ sites and their higher intrinsic reactivities (per site) for aldehyde C=C bond coupling and ring closure reactions, taken together, lead to much higher

aromatic yields on 2D-MFI zeolites than the conventional microporous or mesoporous catalysts.

$C_nH_{2n}O$ ($n = 3-6$) linear aldehydes^[4] undergo three concomitant, kinetically coupled catalytic routes at solid Brønsted acid sites confined within microporous (H-FAU^[4a] and H-MFI zeolites^[4a, 4c]) or mesoporous ($H_4SiW_{12}O_{40}$ ^[4b] or $H_3PW_{12}O_{40}$ ^[5]) dispersed on mesoporous SiO_2) cavities, leading to the formation of unsaturated alkenals, aromatics, alkenes, and dienes. These routes, as shown in Scheme 1, are: (1) *Route A*, inter-molecular C=C bond coupling via aldol condensation-dehydration (Steps 1.1 and 1.2) that increases the carbon chain length to larger, unsaturated alkenals followed by ring closure (Steps 2.1 and 2.2), dehydrogenation (Steps 3.1 and 3.2), and transalkylation (Step 4) reactions that evolve aromatics, (2) *Route B*, transfer hydrogenation (Step 5) between the adsorbed, protonated alkanals and the hydrogen-donors (formed in catalytic *Route A*) that produces alkenes, and (3) *Route C*, monomolecular dehydration reaction that evolves dienes (Step 6).



Scheme 1. Reaction routes for aromatic production from butanals on solid Brønsted acid catalysts (*H-donor* denotes the hydrogen donor in transfer hydrogenation reaction, *Route B*, Step 5).

Among these concomitant reactions, *Route A*, which includes the inter-molecular C=C bond coupling, ring closure, dehydrogenation, and transalkylation steps, is the predominant route. The transfer hydrogenation (*Route B*) occurs favorably only on specific zeolites (e.g., H-FAU^[4a]) and more selectively in

[a] Dr. F. Lin, Prof. Dr. Y-H. Chin
Department of Chemical Engineering and Applied Chemistry
University of Toronto
200 College Street, Toronto, ON, M5S 3E5, Canada
E-mail: cathy.chin@utoronto.ca

[b] J. Zhang, Prof. Dr. D. Liu
Department of Chemical and Biomolecular Engineering
University of Maryland
4418 Stadium Drive, College Park, MD, 20742, USA

large supercages (11.8 Å cage size), whereas the direct alkanal dehydration (*Route C*) remains a minor route (<10% carbon selectivity during butanal reactions on H-MFI, H-FAU, and $H_4SiW_{12}O_{40}$ catalysts at 573 K^[4a]). *Route A*, when occurring at H^+ sites contained in molecularly confined structures, often leads to rapid deactivation,^[6] because aromatics as the desired products are also coke precursors; these aromatics occupy pores and cages, thus reducing the reactant accessibility to acid sites inside the zeolites. The number of accessible H_c^+ sites decreases markedly to <30% on H-MFI (Si/Al = 11.5) and <50% on H-FAU (Si/Al = 15), after steady-state butanal reactions at 573 K for 2 h [1.1 kPa butanal, space velocity = 4 $\mu\text{mol butanal (g}_{\text{cat.}} \text{ s}^{-1})$]^[4a]. In contrast, $H_4SiW_{12}O_{40}$ clusters exhibit a much lower site reduction: the density of unconfined H_{uc}^+ sites on these clusters remains relatively constant [$1.54 \pm 0.32 \text{ mol}_{H^+} (\text{mol}_{H_4SiW_{12}O_{40}})^{-1}$], even after 12 h of reactions at 573 K [1.1-4.4 kPa butanal, space velocity = 7.5-30 $\mu\text{mol butanal (g}_{\text{cat.}} \text{ s}^{-1})$]^[6]. These unconfined H_{uc}^+ sites are, however, much less effective for the sequential ring closure, dehydrogenation, transalkylation, and transfer hydrogenation reactions, leaving the unsaturated, branched alkanal intermediates rather than aromatics as the predominant deoxygenation products.

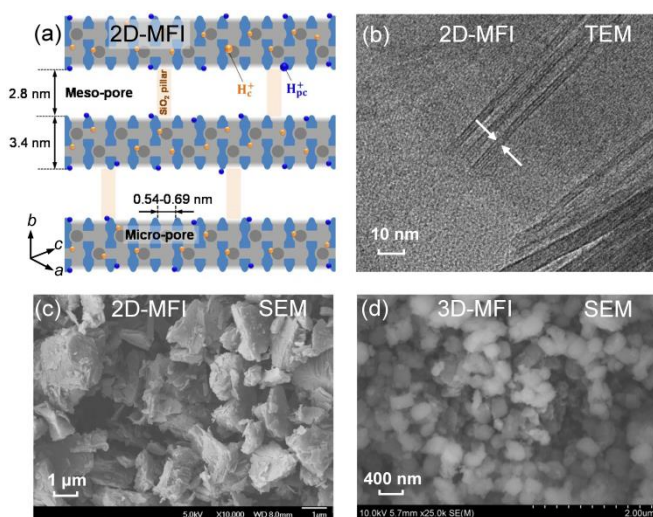


Figure 1. (a) Structure of 2D-MFI [H_c^+ (orange) denotes the H^+ sites confined within the micropores while H_{pc}^+ (dark blue) denotes the partially confined H^+ sites at the intercept between the micro- and meso-pores [Light blue represents the channel walls; light gray represents the channels parallel to the drawing; dark gray represents the channels perpendicular to the drawing], (b) TEM image of 2D-MFI, (c)-(d) SEM images of 2D-MFI and 3D-MFI, respectively.

Next, we synthesized two-dimensional MFI zeolite (2D-MFI) with lamellar layers containing partially confined Brønsted acid sites (Fig. 1a, synthesis procedure in Sec. S5.1) and then correlate their unique structure and site environment to the reactivity and selectivity trends in butanal deoxygenation. Figures 1b and 1c show the SEM and TEM images, respectively, of the lamellar 2D-MFI zeolite (Si/Al ratio = 69). This 2D-MFI contains 3 pentasil layers of microporous sheets with two parallel zigzag channels (in a-c plane) and one directly

perpendicular channel (along b-axis), as illustrated in Figure 1a. The nanosheets have a thickness of about 3.4 nm and a length of about 500 nm (3.4 nm \times 500 nm), stacked in together at an inter-microporous distance of \sim 2.8 nm. In contrast, the conventional three-dimensional H-MFI zeolite (Si/Al ratio = 70, denoted as 3D-MFI, synthesis procedure in Sec. S5.1) contains crystals with comparable dimensions of \sim 200 nm \times \sim 200 nm (Fig. 1d). Table 1 summarizes the density of H_{pc}^+ and H_c^+ sites for these two samples, determined by dimethyl ether titration and 2,6-di-tert-butylpyridine titration^[7] (methods described in Sec. S5.2). Despite having similar Si/Al ratios and total H^+ site densities, the 2D-MFI zeolite contains a much larger fraction of partially confined H_{pc}^+ sites than the 3D-MFI zeolite ($[H_{pc}^+]_0 = 0.081$ vs. $0.007 \text{ mmol g}_{\text{cat.}}^{-1}$); these H_{pc}^+ sites reside at the intercept between the micro- and meso-pores.

Table 1. Properties of lamellar MFI zeolite (2D-MFI) and conventional MFI zeolite (3D-MFI) samples.

Sample	2D-MFI	3D-MFI
Si/Al ratio	69	70
$[H_{\text{total}}^+]_0$ ^a (mmol $\text{g}_{\text{cat.}}^{-1}$)	0.224	0.228
$f_{pc,0}$ ^b	36% ^[8]	3.2%
$[H_{pc}^+]_0$ ^a (mmol $\text{g}_{\text{cat.}}^{-1}$)	0.081	0.007
$[H_c^+]_0$ ^a (mmol $\text{g}_{\text{cat.}}^{-1}$)	0.143	0.221
$[H_{\text{total}}^+]_{2h}$ ^c (mmol $\text{g}_{\text{cat.}}^{-1}$)	0.047	0.022
$[H_{pc}^+]_{2h}$ ^c (mmol $\text{g}_{\text{cat.}}^{-1}$)	0.031	0.007
$[H_c^+]_{2h}$ ^c (mmol $\text{g}_{\text{cat.}}^{-1}$)	0.016	0.015
Dimension	3.4 nm \times 500 nm	200 nm \times 200 nm

^aDensity of total H^+ sites, H_{pc}^+ sites, or H_c^+ sites on fresh catalysts;

^bFraction of H_{pc}^+ sites on fresh catalysts;

^cRemaining site density of total H^+ sites, H_{pc}^+ sites, or H_c^+ sites after 2 h of butanal reactions at 573 K.

Figure 2a compares the time-dependent butanal conversion rates (mass basis) at 573 K between the 2D-MFI ($r_{\text{Butanal,2D}}$) and 3D-MFI ($r_{\text{Butanal,3D}}$) zeolites. Both 2D-MFI and 3D-MFI exhibited similar initial conversion rates, because of near complete butanal conversions (>94% at 5 min on-stream). These rates at near complete conversion, however, do not reflect the intrinsic reactivity. After 2 h reaction, the butanal conversion rate on the 3D-MFI decreased markedly to \sim 10% of its initial value [from $10.9 \mu\text{mol (g}_{\text{cat.}} \text{ s}^{-1})$ to $1.2 \mu\text{mol (g}_{\text{cat.}} \text{ s}^{-1})$]. In contrast, the rates on 2D-MFI decreased, but to a much smaller extent, i.e., to \sim 45% of its initial value after 2 h and \sim 20% after 5 h. These time-dependent profiles confirm that the 2D-MFI remains much more stable than 3D-MFI, which appears to be related to its larger fraction of partially confined H_{pc}^+ sites ($f_{pc,0} = 36\%$ vs. 3.2% on 2D-MFI and 3D-MFI, respectively, Table 1).

Table 1 also compares the densities of accessible H_{pc}^+ and H_c^+ sites on these catalysts after two hours of butanal reactions at 573 K. After 2 h reaction, the Brønsted acid sites confined within the micropores (H_c^+) became largely inaccessible, decreasing by >88%, from 0.143 to 0.016 $\text{mmol g}_{\text{cat.}}^{-1}$ on 2D-MFI and from 0.221 to 0.015 $\text{mmol g}_{\text{cat.}}^{-1}$ on 3D-MFI. In contrast, most of the partially confined H_{pc}^+ sites at the micro- and meso-pore intercepts remained accessible: their site density on 2D-MFI decreased from 0.081 to 0.031 $\text{mmol g}_{\text{cat.}}^{-1}$ and on 3D-MFI remained largely stable, albeit at a much smaller density of 0.007 $\text{mmol g}_{\text{cat.}}^{-1}$. These site titration results, taken together with

the time-dependent reactivities, indicate that partially confined H_{pc}^+ sites, which account for 36% of the total H^+ sites in 2D-MFI, exhibit much higher stability than the confined H_c^+ sites, as they remain accessible and less susceptible to coke poisoning. After 2 h, butanal conversion rates on both the 2D-MFI and 3D-MFI catalysts reached stable values and their rate ratio ($r_{\text{Butanal},2D}/r_{\text{Butanal},3D}$) remained constant (Fig. 2a). Above 2 h, the confined H_c^+ sites became much less effective, because coke accumulation within the micropores renders these sites inaccessible. Thus, the catalytic reactivity reflects predominantly those of the partially confined H_{pc}^+ sites.

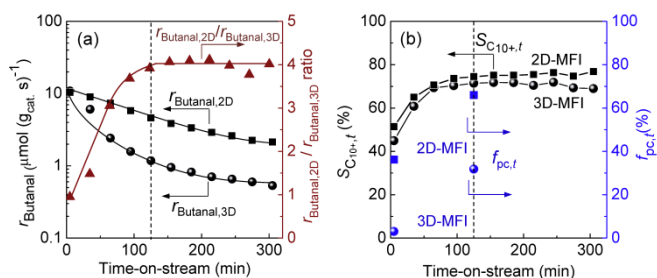


Figure 2. (a) Time-dependent butanal conversion rates (mass basis) on 2D-MFI ($r_{\text{Butanal},2D}$) and 3D-MFI ($r_{\text{Butanal},3D}$) and their rate ratio ($r_{\text{Butanal},2D}/r_{\text{Butanal},3D}$); (b) selectivities to larger C_{10+} aromatics ($S_{C_{10+},t}$) and instantaneous H_{pc}^+ site fraction ($f_{pc,t}$) on 2D-MFI and 3D-MFI, plotted as a function of time-on-stream [$Si/Al = 69-70$, 573 K, 1.1 kPa butanal, space velocity = 33 $\text{mmol}_{\text{butanal}}/(\text{mol}_{H^+} \text{ s})^{-1}$].

Next, we probe the intrinsic reactivity of H_{pc}^+ and H_c^+ sites with a combined site titration and rate measurement method. Figures 3a and 3b show the time-dependent yields of the various products during butanal deoxygenation on 2D-MFI and 3D-MFI, respectively. The aromatics formed via the chain growth route are the predominant, desired products (>70% carbon selectivities). Therefore, we focus on understanding the catalytic roles and contributions of H_c^+ and H_{pc}^+ sites to the formation of these aromatics.

As demonstrated in our previous work,^[4b, 4c] the rate of inter-molecular C=C bond coupling of alkanal (Step 1.1) increases linearly with alkanal pressure, and the adsorbed alkanals are the most abundant surface intermediates during steady-state catalysis. On catalysts containing both the H_c^+ and H_{pc}^+ sites, the overall, extensive rate of inter-molecular C=C bond coupling [$\text{in mol}(\text{g}_{\text{cat}} \text{ s})^{-1}$] at any time-on-stream t , $R_{\text{inter},t}$, relates to the H_c^+ and H_{pc}^+ site densities ($[H_c^+]_t$ and $[H_{pc}^+]_t$) and the respective first-order rate constants on these two types of sites ($k_{\text{inter},c}$ and $k_{\text{inter},pc}$) via (derivation in Sec. S2 of SI):

$$R_{\text{inter},t} = k_{\text{inter},c} P_{\text{Butanal}} [H_c^+]_t + k_{\text{inter},pc} P_{\text{Butanal}} [H_{pc}^+]_t \quad (1)$$

where P_{Butanal} is the butanal partial pressure. Assuming that the reactivity for each type of sites (H_{pc}^+ or H_c^+) remains identical across both samples, the two effective rate constants $k_{\text{inter},c}$ and $k_{\text{inter},pc}$ could be extracted based on the measured values of $R_{\text{inter},t}$, $[H_c^+]_t$, and $[H_{pc}^+]_t$ at steady state (see Sec. S2). These rate constants are shown in Figure 4a, together with that for the

unconfined H_{uc}^+ sites on $H_4SiW_{12}O_{40}$ clusters ($k_{\text{inter},uc,HSiW}$, detailed kinetic study reported previously^[4b]) and mesoporous aluminosilicate Al-MCM-41 ($k_{\text{inter},uc,MCM}$, see Sec. S4 in SI for the detailed kinetic results). The confined H_c^+ sites are much less reactive than the unconfined H_{uc}^+ sites prevalent on $H_4SiW_{12}O_{40}$ clusters and Al-MCM-41 ($k_{\text{inter},c} < k_{\text{inter},uc,MCM} < k_{\text{inter},uc,HSiW}$). We hypothesize that steric constraints imposed by the micro-pores of MFI (5.4 Å × 5.6 Å) destabilize the large, bi-molecular transition state formed during inter-molecular coupling of butanals (kinetic diameter ~5.0 Å).^[9] The partially confined H_{pc}^+ sites are more reactive than both the confined H_c^+ and the unconfined H_{uc}^+ sites ($k_{\text{inter},pc} > k_{\text{inter},uc,HSiW} > k_{\text{inter},uc,MCM} > k_{\text{inter},c}$), apparently because the partially confined environment of these H_{pc}^+ sites promotes the inter-molecular C=C bond coupling reactions, via additional stabilizations of the bi-molecular transition state through van der Waals interactions with the zeolite pore-mouths.^[10] The unconfined H^+ sites on $H_4SiW_{12}O_{40}$ are slightly more active than those on Al-MCM-41 ($k_{\text{inter},uc,HSiW} = 1.6 k_{\text{inter},uc,MCM}$), likely because of the stronger acid strength for the former (deprotonation enthalpy (DPE) = 1105 kJ mol^{-1} vs. 1190-1222 kJ mol^{-1} for $H_4SiW_{12}O_{40}$ ^[11] and aluminosilicate,^[12] respectively). The butanal aldol condensation forms a bulky bi-molecular carbocationic transition state, on which the positive charge is more delocalized than on the mono-molecular carbonationic reactant state (protonated butanal). The transition state formed on a stronger H^+ site (with lower DPE) would require less energy for the positive charge delocalization than on a weaker H^+ site, resulting in a lower activation barrier and higher activity. Similar reactivity trends with acid strength have been reported for Brønsted acid catalyzed methylation, hydride transfer, and isomerization reactions on heteropoly acids and aluminosilicate catalysts.^[13]

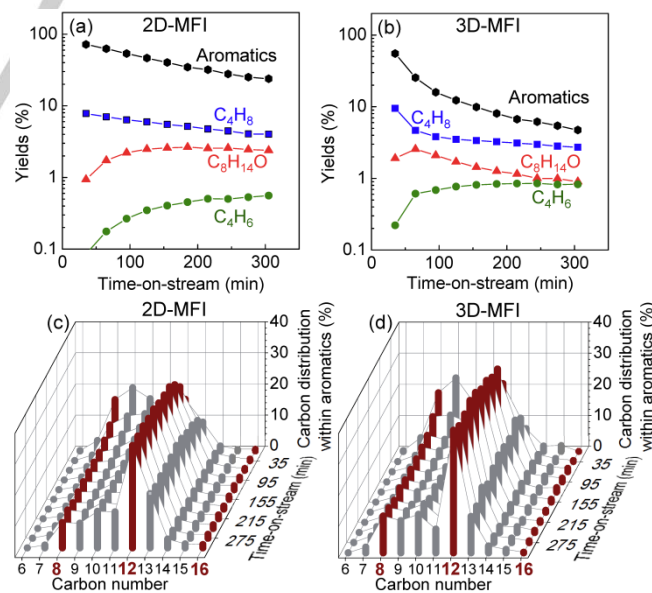


Figure 3. Time-dependent yields of aromatics, light alkene (C_4H_8), diene (C_4H_6), and larger alkenal ($C_8H_{14}O$) during butanal reactions on 2D-MFI (a) and 3D-MFI (b); time-resolved carbon distributions within the aromatic product fraction during butanal reactions on 2D-MFI (c) and 3D-MFI (d) at 573 K [in 3c and 3d, brown: primary ring closure products (C_8 , C_{12} , and C_{16}); gray:

transalkylation products; Si/Al = 69-70, 1.1 kPa butanal, space velocity = 33 $\text{mmol}_{\text{butanal}} (\text{mol}_{\text{H}^+} \text{s}^{-1})^{-1}$.

The local environment of the H^+ sites also influences the sequential ring-closure and transalkylation reactions of *Route A*. Figure 4b compares the carbon selectivities within the products of *Route A* on 2D-MFI, 3D-MFI, $\text{H}_4\text{SiW}_{12}\text{O}_{40}$, and Al-MCM-41 catalysts (573 K, time-on-stream = 2 h). Both 2D-MFI and 3D-MFI exhibit much higher carbon selectivities towards aromatics (>80%) than $\text{H}_4\text{SiW}_{12}\text{O}_{40}$ (~17%) and Al-MCM-41 (~22%), indicating that both the confined H_c^+ and partially confined H_{pc}^+ sites are much more effective than the unconfined H_{uc}^+ sites for the ring-closure reaction.

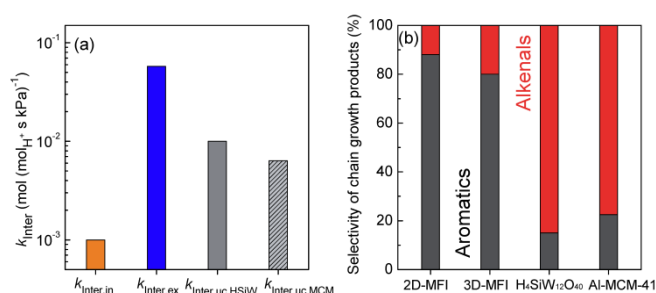


Figure 4. (a) First-order rate constants for inter-molecular C=C bond formation on confined H_c^+ sites ($k_{\text{inter,c}}$) and partially confined H_{pc}^+ sites ($k_{\text{inter,pc}}$) of MFI and on unconfined H_{uc}^+ sites of $\text{H}_4\text{SiW}_{12}\text{O}_{40}$ ($k_{\text{inter,uc,HSiW}}$) and Al-MCM-41 ($k_{\text{inter,uc,MCM}}$) at 573 K (all the rate constants were calculated based on the density of accessible H^+ sites during steady-state butanal reaction); (b) selectivity of aromatics and alkenals ($\text{C}_8\text{H}_{14}\text{O}$) within the chain growth products during butanal reactions on 2D-MFI and 3D-MFI [space velocity = 33 $\text{mmol}_{\text{butanal}} (\text{mol}_{\text{H}^+} \text{s}^{-1})^{-1}$] and on $\text{H}_4\text{SiW}_{12}\text{O}_{40}$ clusters [space velocity = 45 $\text{mmol}_{\text{butanal}} (\text{mol}_{\text{H}^+} \text{s}^{-1})^{-1}$] and Al-MCM-41 [space velocity=180 $\text{mmol}_{\text{butanal}} (\text{mol}_{\text{H}^+} \text{s}^{-1})^{-1}$] at 573 K (2 h, 1.1 kPa butanal, butanal conversion = 55%, 20%, 20%, and 10% on 2D-MFI, 3D-MFI, $\text{H}_4\text{SiW}_{12}\text{O}_{40}$, and Al-MCM-41, respectively).

The primary ring-closure products with 8 and 12 carbon atoms (brown bars in Figs. 3c and 3d) undergo transalkylation on 2D-MFI and 3D-MFI zeolites, leading to aromatics with diverse molecular sizes (C_6 - C_{16+} ; gray bars in Figs. 3c and 3d). The transalkylation reaction, however, essentially does not occur on either $\text{H}_4\text{SiW}_{12}\text{O}_{40}$ clusters or Al-MCM-41 (0% selectivity), because it requires molecularly confined environment.^[4b] Figures 3c and 3d show the carbon distributions of these aromatics produced from 2D-MFI and 3D-MFI as a function of time-on-stream. On both samples, the selectivity to smaller aromatics (C_6 - C_9) decreases and that to larger aromatics (C_{10+}) commensurately increases with time, in response to the gradual poisoning of the confined H_c^+ sites and changes in the H_c^+ -to- H_{pc}^+ site ratio (Table 1). Since aromatics larger than C_9 (e.g., C_{10} naphthalene, kinetic diameter $\sim 6.2 \text{ \AA}$ ^[14]) could not access the micro-pores ($5.4 \text{ \AA} \times 5.6 \text{ \AA}$) of MFI, the confined H_c^+ sites catalyze almost exclusively the formation of smaller aromatics (C_6 - C_9). In contrast, partially confined H_{pc}^+ sites produce both the small and large aromatics (C_6 - C_{16+}). As shown in Figure 2b, the selectivity to C_{10+} aromatics ($S_{\text{C}_{10+,t}}$, defined in Sec. S3) of 2D-MFI and 3D-MFI increases rapidly during the initial 2 h, as the

H_c^+ site density decreases markedly and the instantaneous H_{pc}^+ site fraction ($f_{\text{pc,t}}$) concomitantly increases. After 2 h, the relative abundance of H_{pc}^+ and H_c^+ sites approaches a constant value, as a result, the selectivity $S_{\text{C}_{10+,t}}$ becomes stable. The 2D-MFI exhibits higher $S_{\text{C}_{10+,t}}$ values than 3D-MFI, simply because it has a larger fraction of H_{pc}^+ sites ($f_{\text{pc,2h}} = 66\%$ vs. 32% for 2D-MFI and 3D-MFI, respectively, Fig. 2b).

In summary, 2D-MFI zeolites contain a larger fraction of partially confined H^+ sites (H_{pc}^+) resided at the intercept between the micro- and meso-pores. The partially confined environment around the H_{pc}^+ sites promotes the inter-molecular C=C bond coupling and ring closure reactions of aldehydes by stabilizing the relevant transition states. The unique micro- and meso-pore interfaces allow for effective removal of heavier aromatic products, thus preventing coke formation and mitigating deactivation.

Experimental Section

See supporting information (SI).

Acknowledgments

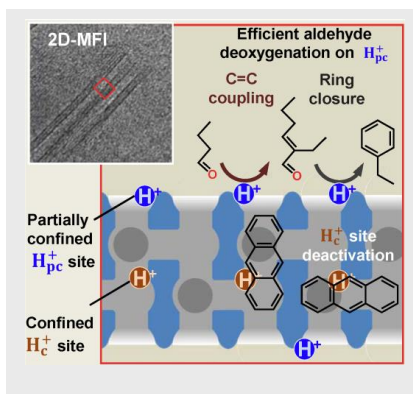
This study was supported by Natural Sciences and Engineering Research Council of Canada (NSERC), Valmet, Abellon CleanEnergy, Canada Foundation for Innovation (CFI); Y.-H. Chin acknowledges Ontario Early Researcher Award Program (ERA), F. Lin acknowledges Hatch Graduate Scholarship for Sustainable Energy Research and Ontario Graduate Scholarship for supports. D. Liu thanks for the support from the National Science Foundation in United States (NSF-CBET 1642405, 1705284 and 1351384). We thank Zhenwei Wu for his help with the kinetic measurements of Al-MCM-41 catalysts.

Keywords: Zeolite nanosheet • Brønsted acid site • aldehyde • C-C coupling • aromatics

- [1] a) K. Tanabea, W. F. Holderich, *Appl. Catal. A* **1999**, *181*, 399-434; b) W. Vermeiren, J. P. Gilson, *Top. Catal.* **2009**, *52*, 1131-1161; c) M. Niwa, N. Katada, K. Okumura, in *The Springer Series in Materials Science, Vol. 141* (Eds.: R.Hull, C. Jagadish, R. M. Osgood, J. J. Parisi, Z.Wang, H.Warlimont), Springer, Heidelberg, **2010**, pp. 1-8.
- [2] a) J. D. Adjaye, N. N. Bakhshi, *Fuel Process. Technol.* **1995**, *45*, 161-183; b) J. D. Adjaye, N. N. Bakhshi, *Fuel Process. Technol.* **1995**, *45*, 185-202.
- [3] a) B. Liu, D. Slocombe, M. AlKinany, H. AlMegren, J. Wang, J. Arden, A. Vai, S. Gonzalez-Cortes, T. Xiao, V. Kuznetsov, P. P. Edwards, *Appl. Petrochem. Res.* **2016**, *6*, 209-215; b) A. Devaraj, M. Vijayakumar, J. Bao, M. F. Guo, M. A. Derewinski, Z. Xu, M. J. Gray, S. Proding, K. K. Ramasamy, *Sci. Rep.* **2016**, *6*, 37586; c) R. B. Rostami, M. Ghavipour, Z. Di, Y. Wang, R. M. Behbahani, *RSC Adv.* **2015**, *5*, 81965-81980; d) M. Guisnet, L. Costa, F. R. Ribeiro, *J. Mol. Catal. A: Chem.* **2009**, *305*, 69-83.
- [4] a) F. Lin, Y.-H. Chin, *J. Catal.* **2016**, *341*, 136-148; b) F. Lin, Y.-H. Chin, *ACS Catal.* **2016**, *6*, 6634-6650; c) F. Lin, Y.-H. Chin, *J. Catal.* **2014**, *311*, 244-256.
- [5] Y. Yang, F. Lin, H. Tran, Y.-H. Chin, *Chem. Cat. Chem.* **2017**, *6*, 287-299.
- [6] K. K. Ramasamy, M. A. Gerber, M. Flake, H. Zhang, Y. Wang, *Green Chem.* **2014**, *16*, 748-760.
- [7] Y. Wu, L. Emdadi, D. Qin, J. Zhang, D. Liu, *Microporous Mesoporous Mater.* **2017**, *241*, 43-51.

- [8] Y. Wu, Z. Lu, L. Emdadi, S. C. Oh, J. Wang, Y. Lei, H. Chen, D. T. Tran, I. C. Lee, D. Liu, *J. Catal.* **2016**, *337*, 177-187.
- [9] A. N. Migués, S. Vaitheeswaran, S. M. Auerbach, *J. Phys. Chem. C* **2014**, *118*, 20283-20290.
- [10] a) B. A. De Moor, M.-F. Reyniers, O. C. Gobin, J. A. Lercher, G. B. Marin, *J. Phys. Chem. C* **2011**, *115*, 1204-1219; b) F. Eder, M. Stockenhuber, J. A. Lercher, *J. Phys. Chem. B* **1997**, *101*, 5414-5419.
- [11] J. Macht, M. J. Janik, M. Neurock, E. Iglesia, *Angew. Chem.* **2007**, *119*, 8010-8014.
- [12] M. L. Sarazen, E. Doskocil, E. Iglesia, *ACS Catal.* **2016**, *6*, 7059-7070.
- [13] D. A. Simonetti, R. T. Carr, E. Iglesia, *J. Catal.* **2012**, *285*, 19-30.
- [14] J. Jae, G. A. Tompsett, A. J. Foster, K. D. Hammond, S. M. Auerbach, R. F. Lobo, G. W. Huber, *J. Catal.* **2011**, *279*, 257-268.

Lamellar MFI zeolite nanosheets (2D-MFI) contain a large fraction of partially confined H^+ sites (H_{pc}^+) residing at the micro- and meso-pore intercepts. These sites are effective for C=C bond coupling and ring closure of aldehydes to produce aromatics. These sheets resemble nanometer-sized plug flow reactor; they allow not only the formation but also effective removal of aromatic products in cascade reactions, thus preventing site occupation by coke and mitigating deactivation.



Fan Lin, Junyan Zhang, Dongxia Liu,
Ya-Huei (Cathy) Chin*

Page No. – Page No.

Cascade Reactions in Tunable
Lamellar Micro-Mesopores for C=C
Bond Coupling and Hydrocarbon
Synthesis